Nanoscale Res Lett (2009) 4:1524–1529
DOI 10.1007/s11671-009-9430-7

NANO EXPRESS

Simple Systematic Synthesis of Periodic Mesoporous Organosilica Nanoparticles with Adjustable Aspect Ratios

Paritosh Mohanty · Kai Landskron

Received: 16 July 2009 / Accepted: 19 August 2009 / Published online: 16 September 2009

Abstract One-dimensional periodic mesoporous organosilica (PMO) nanoparticles with tunable aspect ratios are obtained from a chain-type molecular precursor octaethoxy-1,3,5-trisilapentane. The aspect ratio can be tuned from 2:1 to >20:1 simply by variation in the precursor concentration in acidic aqueous solutions containing constant amounts of triblock copolymer Pluronic P123. The mesochannels are highly ordered and are oriented parallel to the longitudinal axis of the PMO particles. No significant Si–C bond cleavage occurs during the synthesis according to ^{29}Si MAS NMR. The materials exhibit surface areas between 181 and 936 $m^2\ g^{-1}$.

Keywords Periodic mesoporous organosilicas · One-dimensional nanostructures · Synthesis

Introduction

Periodic mesoporous organosilicas (PMOs) have emerged as a diverse class of materials [1–4]. They are composed of O^{2-}-bridged Si–R–Si building units (R = organic group) that build periodic mesoporous frameworks. They can be prepared in surfactant-templated self-assembly processes from organosilanes of the type $(EtO)_3Si–R–Si(OEt)_3$. The presence of the bridging organic groups allows for the use of these organosilanes as single-source precursor without the aid of inorganic co-reactants such as tetraethoxysilane. Thus, a high and homogeneous distribution of organic groups in the channel walls of these materials can be achieved, which renders them with attractive mechanical [5], catalytic [6], sorption [7], and dielectric [8] properties.

One-dimensional (1D) nanostructures, such as nanowires (NWs), nanofibers (NFs), nanotubes (NTs), and nanorods (NRs), are one of the most extensively studied classes of materials in the recent times and many different compositions of 1D nanostructures with many applications ranging from microelectronics [9], to optics [10], to drug-delivery [11], and to bio-detections [12] have been reported. Few reports are available for the synthesis of inorganic periodic mesoporous silica nanofibers. Periodic mesoporous silica nanofibers produced by a "hard-templating" method using porous anodic aluminum oxide as hard templates are reported [13, 14]. The obtained mesoporous silica nanofibers were further used as hard template to synthesize mesoporous carbon nanofibers [15]. Stucky and coworkers synthesized mesoporous silica nanofibers by "soft-templating methods" using cationic surfactants [16, 17]. Chen and coworkers demonstrated the formation of silica nanofibers with a hierarchically helical mesostructure templated by achiral cationic surfactant [18]. One-dimensional purely inorganic periodic mesoporous silicas with lower aspect ratios such as nanorods have also been reported [19]. Periodic mesoporous silica nanorods have recently emerged as vehicles for drug-delivery [20]. Variation in the concentration of the precursor solution has been used as a tool to vary the size of purely inorganic periodic mesoporous silica nanorods [19]. However, to our best knowledge, there is no report in the literature that allows for the systematic variation in the aspect ratio of periodic mesoporous organosilicas over a wide range by a single simple method. One-dimensional periodic mesoporous organosilica particles could potentially be used in drug-delivery applications. The presence of organic bridging groups inside the frameworks may be a potential

P. Mohanty · K. Landskron (✉)
Department of Chemistry, Lehigh University, Bethlehem, PA 18015, USA
e-mail: kal205@lehigh.edu

advantage over purely inorganic systems because of the greater variability of pore surface properties that can be achieved [4].

Generally, the literature about periodic mesoporous organosilicas as nanoparticles (<1,000 nm) is very limited. Terasaki [8] reported the formation of octadecahedral particles from bis(trimethoxysilyl)ethane, and Froeba and coworkers [21] reported uniform PMO spheres with phenylene bridging groups. Jaroniek reported PMOs with multiple bridging groups and spherical morphologies [22, 23]. While the PMO particle sizes and shapes in these reports are uniform, their diameter is larger than 1 μm in all cases. Recently, we described the first example of a periodic mesoporous organosilica with very uniform rice-shaped nanoparticles having aspect ratios of ca. 3:1. The PMO was prepared using the organosilane octaethoxy-1,3,5-trisilapentane (***1***) as single-source precursor [24]. Herein, we report that PMO nanoparticles with tunable aspect ratios can be synthesized simply by systematic variation in the concentration of (***1***) in acidic solutions containing surfactant templates. The particles obtained are highly uniform, and the aspect ratio can be systematically varied over a wide range from 2:1 to >20:1.

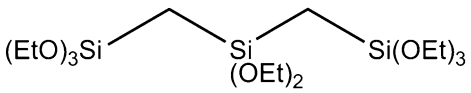

1

Results and Discussion

PMO nanofibers (PMO NFs) were obtained when a reaction mixture of 0.76 mmol ***1***: x ($x = 51$ mmol NaCl: 0.11 mmol P123: 33.6 mmol HCl: 310 mmol H_2O) was used. The PMO NFs have a diameter of ~100 nm. The length of as-synthesized NFs extends to tens of μm according to TEM (Fig. 1).

Upon extraction of the NFs, their length is somewhat reduced to about 2–5 μm according to SEM (Fig. 2a). This indicates high mechanical fragility of the NFs, which is more pronounced in the porous state compared to the as-synthesized state. From the TEM (Fig. 3a) and HRTEM images of extracted NFs (Fig. 3b), it can be clearly seen that the mesochannels run strictly parallel to the longitudinal direction of the NFs. It can be seen from Fig. 3b that the PMO NFs consist of ca. 10 mesochannels. The wall thickness measured from the HRTEM image was ~7 nm, and the pore diameter could be estimated to be ~4 nm. The periodicity of the NFs was confirmed by SAXS as shown in Fig. 4a. An intense reflex was observed at 0.75° 2θ with an interplanar spacing d of 11.7 nm. The lattice parameter a was calculated to be 13.5 nm. The highly ordered arrangement of the mesopores investigated by SAXS confirms periodicity of mesopores in the organosilica NFs.

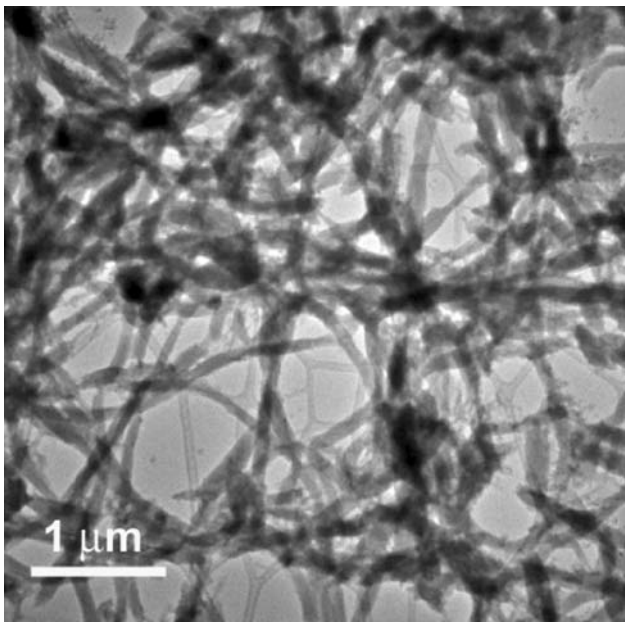

Fig. 1 TEM image of the PMO NFs (as-synthesized)

The N_2 adsorption–desorption isotherm of the NF sample (Fig. 5a) shows a type-IV isotherm with a capillary condensation at P/P_0 of 0.45–0.7. This suggests that the NF sample has uniform mesoporous channels. The BET surface area and total pore volume were calculated to be 181 $m^2\ g^{-1}$ and 0.406 $cm^3\ g^{-1}$, respectively. The pore size distribution (PSD) calculated from the desorption branch of the isotherm using the BJH method was 4.9 nm (Fig. 6a). The structural parameters of the physicochemical property of the NFs are summarized in the Table 1 (row four).

In order to prove the existence of the organic groups in the sample after the template removal, we have studied the NFs by ^{13}C and ^{29}Si MAS NMR spectroscopy. Figure 7a shows the ^{13}C MAS NMR spectrum of the extracted NF sample. Only one signal at 4 ppm was observed. This demonstrates the presence of the CH_2 groups. Small signals around 65 ppm indicate that a small amount of template remains in the pores presumably due to the high aspect ratio of the particles. The ^{29}Si MAS NMR spectrum (Fig. 8a) showed the presence of both D sites and T sites. The signals observed between −8 and −32 ppm can be assigned to D sites, while the signals between −39 and −75 ppm can be assigned to T sites. The signals around −17 and −24 ppm represent the D_1 and the D_2 sites, respectively. The signals at −51, −56, and −64 ppm are from the T_1, T_2, and T_3 sites, respectively. The presence of the D and T sites in the ^{29}Si MAS NMR and the presence of only signal at 4 ppm in the ^{13}C MAS NMR spectrum confirms that

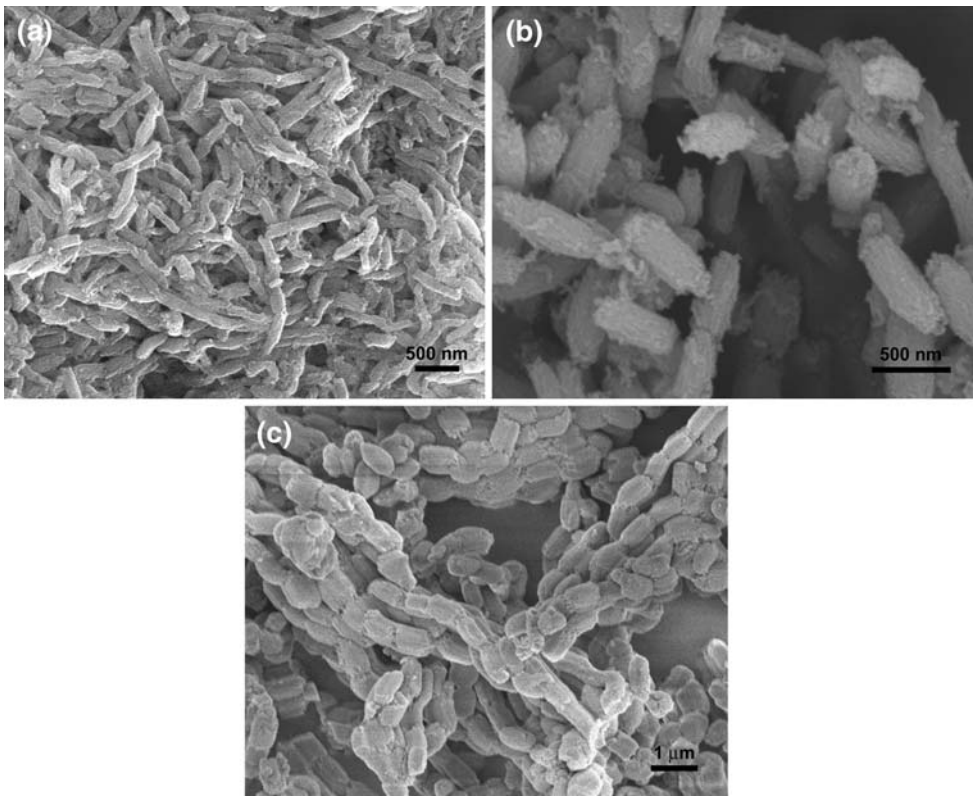

Fig. 2 SEM images of extracted PMO nanostructures; *a* NFs, *b* NRs, and *c* NEs

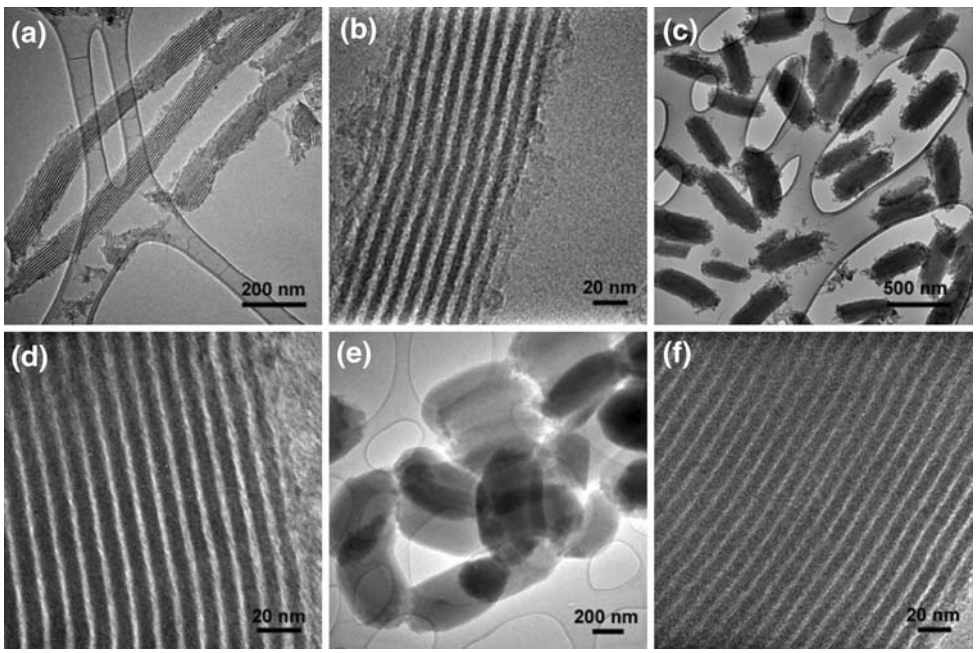

Fig. 3 TEM and HRTEM images of extracted PMO nanostructures; *a* and *b* NFs, *c* and *d* NRs, *e* and *f* NEs

practically no Si–C bonds have cleaved neither during the synthesis nor during the template removal process.

In an attempt to rationalize the formation process of the 1D nanostructures, we performed analogous experiments by changing the concentration of the precursor. On increasing the concentration of the precursor from 0.76 to 1.01 mmol/x, nanorods (NRs) were observed under analogous experimental conditions. It was shown by SEM (Fig. 2b) and TEM (Fig. 3c, d) images that the NRs have diameters of ~200 nm and lengths of ~800 nm. The aspect ratio was decreased

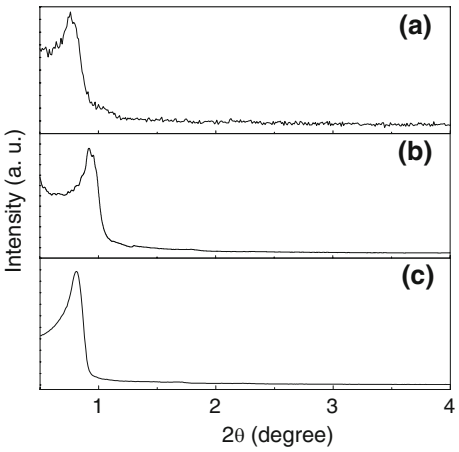

Fig. 4 SAXS patterns of PMO nanostructures *a* NFs, *b* NRs, and *c* NEs

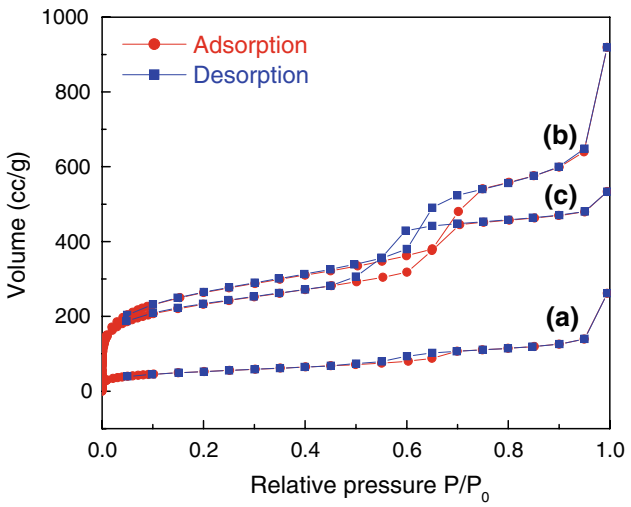

Fig. 5 N_2 isotherm of PMO nanostructures *a* NFs, *b* NRs, and *c* NEs

from >20:1 for the NFs to 4:1 for the NRs. Thus, the thickness of the particle increases at the expense of the length. The wall thickness calculated from the HRTEM image was ~5 nm (pore diameter ca. 4 nm). Similar to the NFs, the NR nanochannels run parallel to the longitudinal direction. The SAXS pattern (Fig. 4b) along with the HRTEM image

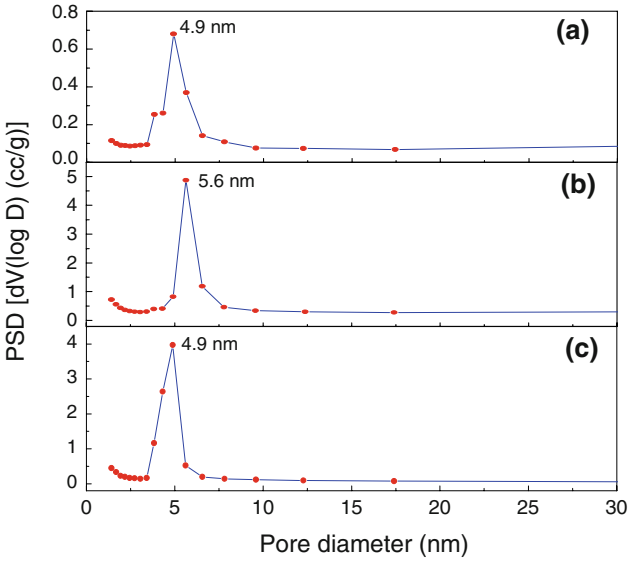

Fig. 6 PSD calculated by BJH method of extracted PMO nanostructures; *a* NFs, *b* NRs, and *c* NEs

confirms the periodicity of the mesopores in the NR sample. The NRs have a type-IV N_2 adsorption–desorption isotherm (Fig. 5b) with a BET surface area of 936 m^2 g^{-1} and total pore volume of 1.425 cm^3 g^{-1}. The BJH PSD was calculated to be 5.6 nm (Fig. 6b). Furthermore, observation of the D and T sites in the ^{29}Si MAS NMR (Fig. 8b) and only one signal at 4 ppm in the ^{13}C MAS NMR (Fig. 7b) confirm the preservation of the organic groups during the synthesis as well as the template removal process. In comparison with the nanofibers, the template can be removed more effectively due to the shorter aspect ratios and the shorter diffusion paths.

On further increasing the concentration of the precursor to 3.04 mmol/x, a nanoegg (NE) type morphology with aspect ratios of ca. 2:1 was observed as can be seen by SEM (Fig. 2c) and TEM (Fig. 3e). As this concentration is even higher than the previously used concentration that gave particles with aspect ratios of 3:1 [24], the lower aspect ratios for PMO NEs are expected. In this case, the decrease in the aspect ratio of the NEs when compared to the NRs does not occur at the expense of the length but is

Table 1 Physicochemical data for PMO nanoparticles

Sample	*d*-spacing (nm)	BET surface area (m^2/g)	Pore volume (cm^3/g)[a]	Pore diameter (nm)	Wall thickness (nm)[b]
Nanoeggs	10.9	815	0.827	4.9	7.7
Nanorice	10.4	753	0.620	4.3	6.1
Nanorods	9.8	936	1.425	5.6	5.7
Nanofibers	11.7	181	0.406	4.9	8.6

[a] Total pore volume obtained from the volume of N_2 adsorbed at P/P_0 of 0.99

[b] Wall thickness estimate = lattice parameter a_0 − pore diameter; $a_0 = 2d_{100}/\sqrt{3}$

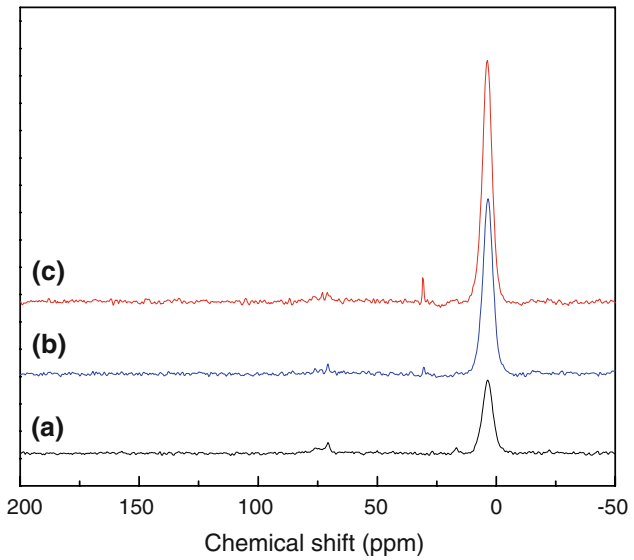

Fig. 7 ^{13}C MAS NMR spectra of PMO nanostructures *a* NFs, *b* NRs, and *c* NEs

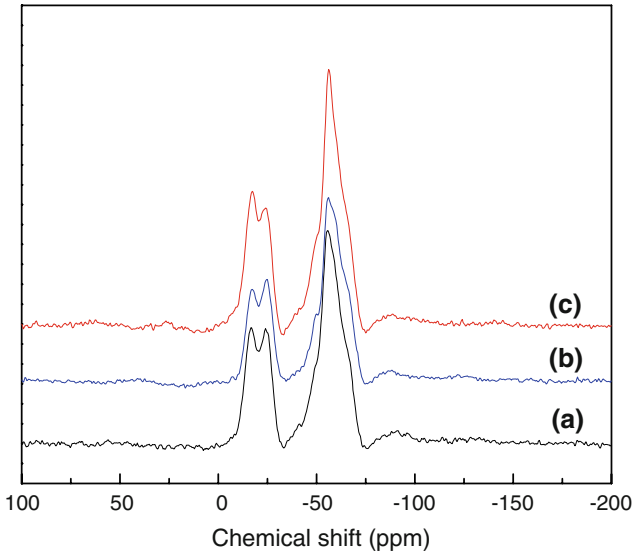

Fig. 8 ^{29}Si MAS NMR spectra of PMO nanostructures *a* NFs, *b* NRs, and *c* NEs

solely due to the increase in the diameter. In comparison with the PMO nanorice, the NE particles are slightly longer (800 vs. 600 nm) [24]. Overall, there is a clear trend that the diameter of the particles increases with the aspect ratio (NF: 100 nm, NR: 200 nm, nanorice: 300 nm, NE: 400 nm). The SEM image (Fig. 2c) shows that a significant number of NEs are interconnected to neck-laced chains. This suggests that the nanoeggs do not form independently from each other. Possibly, the formation of a nanoegg induces the nucleation of further nanoeggs at the nanoegg tips. An individual PMO NE is formed by breaking the chains at the necks, which is presumably the mechanically weakest point. Such necklaces have not been observed for the nanorod structures. Assuming the same formation mechanism as for the nanoeggs, the absence of chains for NRs may be due to the fact that these structures have smaller particle diameters, and thus, practically all chains have been broken at the necks to form individual particles during synthesis.

Similar to the NFs and NRs, the mesopores in the NEs are periodically ordered as can be seen by the HRTEM image (Fig. 3f) and the SAXS pattern (Fig. 4c). The ^{13}C (Fig. 7c) and ^{29}Si (Fig. 8c) MAS NMR spectroscopy of the NE sample further confirm the absence of the template and the presence of the organic groups. The sample has a type-IV isotherm with a BET surface area of 815 $m^2\ g^{-1}$ and pore volume of 0.827 $cm^3\ g^{-1}$. The BJH PSD was calculated to be 4.9 nm (Fig. 6c).

The NR sample has a maximum surface area among the three samples (Table 1), while the surface area of the nanorice and the nanoeggs are slightly smaller. This can be explained by the fact that the nanorods have the thinnest pore walls and the largest pore diameters (Table 1). The NF sample has by far the lowest surface area of 181 $m^2\ g^{-1}$. The NFs have the largest pore wall thickness of the three nanostructures, but this alone may not be the only contributor to the strong decrease of surface area. The very high aspect ratio and the one-dimensional pore systems should make the PMO NFs more prone to pore-clogging in comparison with the NEs and NRs. In principle, only two clogs are sufficient to make a mesochannel inaccessible. This is further supported by the fact that it was not possible to fully extract the surfactant template from the PMO NFs, while practically all templates were extracted from the other samples. Pore-clogging in SBA-15 type materials has been observed previously when the synthesis temperature was kept near room temperature [25]. Similar conditions have been applied for the synthesis of the PMO NFs.

A question is what guides the formation of the one-dimensional PMO nanostructures. Therefore, we have investigated whether the formation of the one-dimensional nanostructures is unique to the octaethoxy-1,3,5-trisilapentane precursor. To do so, we have used tetraethoxysilane and bis-(triethoxysilyl)methane as precursor molecules under otherwise identical synthesis conditions. While also in these cases, it was observed that periodic mesoporous materials formed no well-defined morphology. There is experimental evidence that the special structure of octaethoxy-1,3,5-trisilapentane precursor molecule guides the formation of the one-dimensional periodic mesoporous organosilica particles. The concentration dependence of the aspect ratio becomes plausible when considering that the nucleation of new particles is generally disfavored at lower concentrations.

Experimental

An acid-catalyzed surfactant-templating sol–gel technique was used for the synthesis of the periodic mesoporous organosilica (PMO) nanostructures. Octaethoxy-1,3,5-trisilapentane (Gelest, Inc.) was used as the organosilica source. For a typical synthesis, to a mixture of 3 g NaCl, 0.65 g of Pluronic P123 (BASF), 16.8 g of 2 M HCl, and 5.6 g H_2O, m g ($m = 0.36$, 0.48, and 1.44) of octaethoxy-1,3,5-trisilapentane was added dropwise under vigorous stirring. The mixture was continuously stirred for another 24 h under the formation of a white solid. The solid particles were centrifuged off. The template was extracted by stirring the solid in a mixture of 100 g of acetone and 10 g of 2 M HCl. The extracted particles were filtered off and dried at 80 °C for 1 h.

The SEM images of the specimen were taken on a Hitachi S-4300 SEM. The TEM samples were studied by a JEOL JEM-2000 electron microscope operated at 200 kV. Samples for the TEM analysis were prepared by dispersing the particles in acetone and dropping a small volume of it onto a holey carbon film on a copper grid. SAXS patterns were obtained using a Rigaku Rotaflex diffractometer with a Cu K_α radiation source ($\lambda = 0.15405$ nm). The N_2 adsorption–desorption isotherm was measured at 77 K using Autosorb-1 instrument (Quantachrome). Prior to the measurement, the samples were outgassed at 120 °C overnight. The ^{13}C and ^{29}Si NMR spectra were obtained at 59.616 MHz (silicon-29) or 75.468 MHz (carbon-13) on a General Electric NMR Instruments model GN-300 equipped with a Doty Scientific 7 mm MAS probe. One-pulse spectra were measured with a 1.0 μs pulse length (corresponding to a 20° tip angle) and a relaxation delay of 5.0 s (silicon) or 10 s (carbon) for 16,000–29,000 acquisitions while spinning at typically 5.0 kHz. Additional spectra (not shown) were acquired to assure quantitative NMR signal intensities. Proton decoupling during the 40 ms acquisition time was performed with a continuous 70 kHz radiofrequency field at 300.107 MHz. The time domain signal was conditioned with a Gaussian line-broadening function equivalent to 50 Hz prior to Fourier transformation.

Acknowledgments Dr. James E. Roberts is gratefully acknowledged for MAS NMR measurements. We further thank Dr. Chris Kiely and Dr. Dave Ackland for generously supporting our TEM investigations. Dr. G. Slade Cargill is gratefully acknowledged for supporting our X-ray diffraction experiments.

References

1. T. Asefa, M.J. MacLachlan, N. Coombs, G.A. Ozin, Nature **402**, 867 (1999)
2. S. Inagaki, S. Guan, Y. Fukushima, T. Ohsuna, O. Terasaki, J. Am. Chem. Soc. **121**, 9611 (1999)
3. B. Melde, B. Holland, C. Blanford, A. Stein, Chem. Mater. **11**, 3302 (1999)
4. B.D. Hatton, K. Landskron, W. Whitnall, D.D. Perovic, G.A. Ozin, Acc. Chem. Res. **38**, 305 (2005)
5. K. Landskron, B.D. Hatton, D.D. Perovic, G.A. Ozin, Science **302**, 266 (2003)
6. D. Dube, M. Rat, F. Beland, S. Kaliaguine, Microporous Mesoporous Mater. **111**, 596 (2008)
7. H. Wu, C. Liao, Y. Pan, C. Yeh, H. Kao, Microporous Mesoporous Mater. **119**, 109 (2009)
8. S. Guan, S. Inagaki, T. Ohsuna, O. Terasaki, J. Am. Chem. Soc. **122**, 5660 (2000)
9. A. Javey, S. Nam, R.S. Friedman, H. Yan, C.M. Lieber, Nano Lett. **7**, 773 (2007)
10. R. Agarwal, C.M. Lieber, Appl. Phys. A **85**, 209 (2006)
11. J.B. Melanko, M.E. Pearce, A.K. Salem, Biotechnol. Pharm. Aspects **10**, 105 (2009)
12. G. Gruner, Anal. Bioanal. Chem. **384**, 322 (2006)
13. K. Jin, B. Yao, N. Wang, Chem. Phys. Lett. **409**, 172 (2005)
14. A. Yamaguchi, H. Kaneda, W. Fu, N. Teramae, Adv. Mater. **20**, 1034 (2008)
15. W.S. Chae, M.J. An, S.W. Lee, M.S. Son, K.H. Yoo, Y.R. Kim, J. Phys. Chem. B **110**, 6447 (2006)
16. J. Wang, C.K. Tsung, W. Hong, Y. Wu, J. Tang, G.D. Stucky, Chem. Mater. **16**, 5169 (2004)
17. C.K. Tsung, W. Hong, Q. Shi, X. Kou, M.H. Yeung, J. Wang, G.D. Stucky, Adv. Funct. Mater. **16**, 2225 (2006)
18. J. Wang, W. Wang, P. Sun, Z. Yuan, B. Li, D. Ding, T. Chen, J. Mater. Chem. **16**, 4117 (2006)
19. X. Ji, K. Lee, M. Monjauze, L. Nazar, Chem. Comm. **36**, 4288 (2008)
20. S. Giri, B. Trewyn, M. Stellmaker, V. Lin, Angew. Chem. Int. Ed. **44**, 5038 (2005)
21. V. Rebbin, R. Schmidt, M. Froeba, Angew. Chem. Int. Ed. **45**, 5210 (2006)
22. E. Cho, D. Kim, M. Jaroniec, J. Phys. Chem. C **112**, 4897 (2008)
23. E. Cho, D. Kim, M. Jaroniec, Langmuir **23**, 11844 (2007)
24. P. Mohanty, K. Landskron, Nanoscale Res. Lett. **4**, 169 (2009)
25. P. Van Der Voort, P.I. Ravikovitch, A.V. Neimark, M. Benjelloun, E. Van Bavel, K.P. De Jong, B.M. Weckhuysen, E.F. Vansant, Stud. Surf. Sci. Catal. **141**, 45 (2002)